processes

MDPI

Article

Anodic Behavior of Hafnium in Anhydrous Electrodissolution-Coupled Hafnium Alkoxide Synthesis

Shuai Li [1], Shenghai Yang [1], Pengfei Zhao [1], Yongming Chen [1], Chaobo Tang [1], Yanqing Lai [1], Chaoyong Deng [2] and Changhong Wang [1,*]

[1] School of Metallurgy and Environment, Central South University, Changsha 410083, China
[2] Ximei Resources Limited Company, Qingyuan 513000, China
* Correspondence: changhong.wang@csu.edu.cn

Abstract: The electrodissolution-coupled hafnium alkoxide ($Hf(OR)_4$, R is alkyl) synthesis (EHS) system, which has significant environmental and economic advantages over conventional thermal methods, serves as a promising system for green and efficient $Hf(OR)_4$ electro-synthesis. The EHS system is operated based on the simultaneous heterogeneous reactions of hafnium dissolution and ethanol dehydrogenation, as well as the spontaneous solution-based reaction of Hf^{4+} and OR^-. Employing green ethanol and Hf as feedstocks, the anodic hafnium corrosion/dissolution electrochemical behavior of the Et_4NCl or Et_4NHSO_4 based anhydrous system was investigated through electrochemical measurements combined with SEM observations. The results demonstrated that the Et_4NCl-based anhydrous ethanol system exhibited an efficient mechanism of passive film pitting corrosion breakdown and metal hafnium dissolution, while the Et_4NHSO_4-based anhydrous ethanol system reflected the weak corrosion mechanism of the anodic hafnium under the passive film. The polarization resistance of the Et_4NCl system was dramatically lower than that of the Et_4NHSO_4 system, which indicated that the Et_4NCl system had superior anodic hafnium corrosion performance compared to the Et_4NHSO_4 system. Overall, the investigation of the electrochemical behaviors of anodic hafnium corrosion/dissolution provides theoretical guidance for the efficient operation of EHS electrolysis.

Keywords: hafnium; anhydrous ethanol; tetraethylammonium chloride; tetraethylammonium bisulfate; electrocatalytic corrosion; mechanism; polarization resistance

Citation: Li, S.; Yang, S.; Zhao, P.; Chen, Y.; Tang, C.; Lai, Y.; Deng, C.; Wang, C. Anodic Behavior of Hafnium in Anhydrous Electrodissolution-Coupled Hafnium Alkoxide Synthesis. *Processes* **2023**, *11*, 564. https://doi.org/10.3390/pr11020564

Academic Editor: Fiseha Tesfaye

Received: 20 January 2023
Revised: 6 February 2023
Accepted: 9 February 2023
Published: 13 February 2023

1. Introduction

Hafnium alkoxides ($Hf(OR)_4$, R is alkyl) serve as excellent precursors for high dielectric constant gate hafnium oxide (HfO_2) [1–4] with favorable controllability, high stability, high dielectric constant, and superior compatibility [5]. Atomic layer deposition (ALD) based preparation [6,7] of hafnium oxide from $Hf(OR)_4$ has many desirable advantages over metal chlorides, such as high reactivity, low deposition temperature, and no risk of chlorine contamination of the films [8,9], that accord it a bright future in next-generation semiconductor integration.

Currently, the "thermal halide synthesis" approach via the reaction $HfCl_4+4ROH+4NH_3 \xrightarrow{C_6H_6} Hf(OR)_4+4NH_4Cl$, is predominant for the preparation of $Hf(OR)_4$ [10], but its undesired environmental challenges and economic burden are hindering its widespread industrial application [11]. That is because the conventional halide synthesis emits NH_4Cl solid waste, toxic gases such as chlorine and benzene, and significant CO_2 emissions and produces various side reactions with low thermal efficiency and low yields of $Hf(OR)_4$ (less than 70%) [10]. Thermal halide synthesis involves four steps: pretreatment, chemical synthesis, suction filtration, and distillation purification. The synthesis process utilizes benzene (C_6H_6) as a diluent and improves the reaction rate by adding ammonia. However, this also results in forming NH_4Cl solid waste and releasing toxic substances such as

chlorine gas and benzene during the chlorination and evaporation steps. Thermal halide synthesis requires the combustion of hydrocarbons to sustain its endothermic reaction, which results in a large CO_2 emission footprint. In addition, the cumbersome synthesis process, the large investment in equipment, and the low controllability of the synthesis reaction resulting in unsatisfactory yields and efficiencies of $Hf(OR)_4$ also make the overall economics of thermal synthesis undesirable.

To achieve green and efficient $Hf(OR)_4$ synthesis, we proposed a prospective electrodissolution-coupled $Hf(OR)_4$ synthesis (EHS) system, which employed anhydrous alcohol as the solvent and metal Hf as the feedstock, based on anodic Hf corrosion/dissolution, cathodic ethanol dehydrogenation and the spontaneous binding reaction of Hf^{4+} with OR^-. The design concepts of the EHS system are derived from the field of efficient electro-refining based on hydrometallurgy [12,13] and renewable energy for green hydrogen preparation [14,15]. Thus, during the Faraday-driven EHS process, electricity is applied directly to the target material to accurately regulate the charge transfer and promote its efficient electro-synthesis without solid or toxic waste emissions and with only negative carbon hydrogen as a by-product [16]. Compared with conventional thermal methods, EHS systems present the environmental and economic advantages of no solid waste, no toxic emissions, and high efficiency. In our previous works, we investigated the electrochemical behavior and processes of cathodic dehydrogenation and anodic hafnium dissolution in tetraethylammonium chloride (Et_4NCl)-based and tetraethylammonium bisulfate (Et_4NHSO_4)-based EHS systems to reveal the operational mechanism of the EHS process [17,18]. We investigated the technical viability and economic applicability of tetraethylammonium chloride (Et_4NCl)-based EHS systems, which demonstrated waste-free and efficient production of high-purity Hf ethoxide [$Hf(OC_2H_5)_4$], with an electric energy requirement of 2.92 kWh_e/kg $Hf(OC_2H_5)_4$, anodic Faradaic efficiency of 94.29%, cathodic Faradaic efficiency of 92.75%, $Hf(OC_2H_5)_4$ yield of 93.09% and green H_2 yield of 98.51%. Furthermore, the electrochemical behavior of the EHS process in the tetraethylammonium hydrogen sulfate (Et_4NHSO_4)-based system revealed that the efficient operation of the Et_4NHSO_4-based EHS process is severely hindered by the weak anodic hafnium dissolution/corrosion occurring within the spontaneously formed passive film, indicating that the Et_4NHSO_4-based EHS process requires a solution to the anodic process inefficiency challenge to make it technically feasible. The results indicated that the anodic hafnium corrosion/dissolution based on passive film breakdown served as the dynamically restrictive process for the entire EHS system. Since the anodic hafnium corrosion/dissolution directly affected the yield, energy consumption, and other critical technical parameters of the EHS system, it was of great significance in guiding the efficient operation and systematic engineering application of the EHS system. However, the existing works have yet to conduct a relevant systematic investigation on the anodic hafnium corrosion/dissolution of the Et_4NCl-based and Et_4NHSO_4-based EHS systems.

In this work, we explored the anodic Hf corrosion/dissolution mechanism and kinetics in Et_4NCl and Et_4NHSO_4 based anhydrous systems that used green ethanol as solvent and Hf metal as oxidation-active medium. Firstly, we investigated the anodic behavior of Hf in the Et_4NCl-based anhydrous ethanol system, which revealed a pitting corrosion mechanism and kinetics. The results demonstrated that the Et_4NCl system exhibited an efficient mechanism of passive film pitting corrosion breakdown and metal Hf dissolution. Important kinetic parameters such as anodic Tafel slope (b_a) and corrosion rate (v_{corr}) extracted based on the Butler–Volmer equation indicated that higher temperature and Et_4NCl concentration facilitated Hf pitting kinetics and charge transfer and increased the pitting corrosion activity, thus promoting the anodic Hf corrosion/dissolution. Then, we proceeded to explore the anodic behavior of Hf in the Et_4NHSO_4-based anhydrous ethanol system, which revealed a corrosion mechanism under the passive film and related passive kinetics. The $|m|$ related to the passive rate was extracted to quantify the anodic Hf corrosion kinetics. The results indicated that the increase in the applied potential E_{ap} enhanced the adsorption of aggressive anions (HSO_4^-) on the surface of the passive film, which exacerbated the dissolution of the passive film. Finally, we compared Hf corrosion

between Et_4NCl and Et_4NHSO_4 systems by polarization resistance analysis. The results demonstrated that the improvement in external conditions reduced the kinetic hindrance to anodic Hf corrosion/dissolution and thus facilitated the Hf corrosion/dissolution reaction. Under the same conditions, the polarization resistance of the Et_4NCl system was dramatically lower than that of the Et_4NHSO_4 system, which indicated that the kinetic hindrance to anodic Hf corrosion/dissolution was at a lower level in the Et_4NCl system than in the Et_4NHSO_4 system, making it easier for Hf corrosion/dissolution to occur. It further confirmed that the Et_4NCl system had superior anodic Hf corrosion performance compared to the Et_4NHSO_4 system. The acquired fundamental mechanism and kinetics data would provide important implications and insights for efficient anodic Hf corrosion/dissolution in the EHS process.

2. Theoretical Mechanism of Electro-Synthesis in the EHS System

The electro-synthesis process in the electrodissolution-coupled $Hf(OR)_4$ synthesis (EHS) system employs ethanol and metal Hf as feedstocks to prepare crude $Hf(OR)_4$, which consists of synergistic heterogeneous reactions of cathodic dehydrogenation and anodic Hf dissolution and solution-based combination reaction (Figure 1). Specifically, for the electro-synthesis of hafnium ethoxide [$Hf(C_2H_5O)_4$], anodic Hf corrosion/dissolution is an irreversible reaction based on the dissolution of Hf atoms from the active sites or defective regions under the naturally formed passive film into the electrolyte in the form of Hf^{4+} cations via (R1). Ethanol (C_2H_5OH) adsorbed on the cathode surface is dehydrogenated via (R2) to form a $C_2H_5O^-$ anion, which inter-migrates with the Hf^{4+} cation and spontaneously forms $Hf(C_2H_5O)_4$ via (R3).

$$Hf \rightarrow Hf^{4+} + 4e^- \quad \text{(R1)}$$

$$2C_2H_5OH + 2e^- \rightarrow 2C_2H_5O^- + H_2\uparrow \quad \text{(R2)}$$

$$Hf^{4+} + 4C_2H_5O^- \rightarrow Hf(C_2H_5O)_4 \quad \text{(R3)}$$

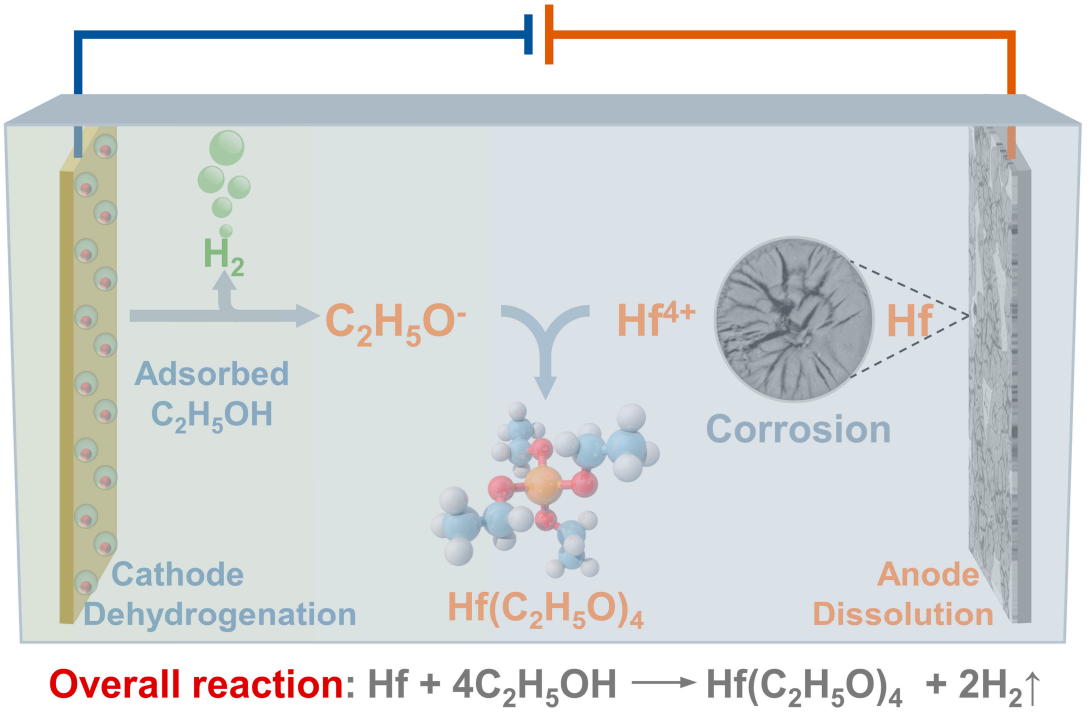

Figure 1. Theoretical mechanism of $Hf(OR)_4$ electro-synthesis process based on anodic corrosion/dissolution.

3. Experimental Section

3.1. Materials

Ethanol (CH_3CH_2OH, ≥99.5%), acetonitrile (CH_3CN, ≥99.8%), tetraethylammonium chloride (Et_4NCl, ≥99%), tetraethylammonium bisulfate (Et_4NHSO_4, ≥99%), and other reagents used in all experiments were purchased from Aladdin without further purification.

3.2. Electrochemical Measurement

The electrochemical measurement equipment for the anodic Hf corrosion/dissolution behaviors of the EHS system consists of the CHI660E electrochemical workstation (Shanghai CH Instrument Company, Shanghai, China) and a typical three-electrode system with temperature adjustment by a thermostatic water bath, which is illustrated as Figure 2. Among them, a hafnium electrode (HE, working area of 0.047 cm^2) with Hf metal wire sealed in a PTFE rod served as the working electrode for the investigation of anodic corrosion/dissolution behaviors, and a Pt sheet electrode (PE) with an area of 1 cm^2 and a saturated calomel electrode (SCE) served as the auxiliary electrode and reference electrode, respectively.

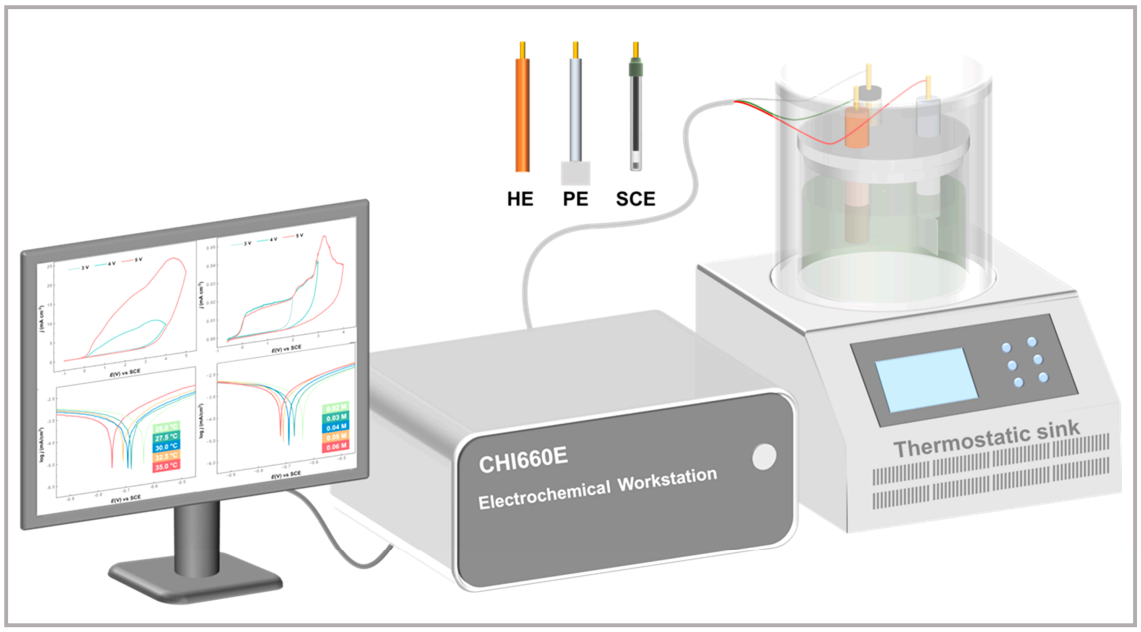

Figure 2. Schematic diagram of the electrochemical measurement equipment for the three-electrode system of the anodic Hf corrosion/dissolution in the EHS system. Working, auxiliary and reference electrodes are hafnium electrode (HE), platinum electrode (PE) and saturated calomel electrode (SCE), respectively.

The electrolyte was composed of a mixed solution of ethanol and acetonitrile (V/V = 1:1) containing Et_4NCl or Et_4NHSO_4 (0.02 to 0.10 M), into which high-purity nitrogen gas was fed to remove the dissolved oxygen. Prior to each electrochemical measurement, the working electrode was subjected to a series of treatments of metallographic sandpaper (coarse-P1200 to fine-P3500) polishing, anhydrous ethanol washing, ultrasonic treatment, and advanced mirror tissue wiping to remove loose adsorbed ions. The prepared electrodes were assembled and immersed in the purged electrolyte until the open circuit potential remained stable.

Cyclic voltammetry (CV) was measured at different potentials (−1 V~3 V, 4 V, and 5 V for Et_4NCl; −0.65 V~3 V, 4 V, and 5 V for Et_4NHSO_4), which were corrected by IR drop compensation adopting the current interrupt (CI) method. The chronoamperometric measurements (CA) were obtained at different anodic applied potentials by constant potential (2.0~5.6 V). To quantify the effect of applied potentials (E_{ap}) on anodic Hf corrosion

kinetics, we converted the *j*–*t* curves to the logarithmic scale and extracted the $|m|$ related to the passive rate. The anodic Hf corrosion kinetic parameters such as anodic Tafel slope (b_a), corrosion rate (v_{corr}), and polarization resistance (R_p) were obtained based on the Butler–Volmer equation [19] and Stern–Geary equation [20]. Furthermore, the anodic Hf corrosion/dissolution behaviors of the Et_4NCl or Et_4NHSO_4 based anhydrous system were investigated by combining SEM (TESCAN Vega3 SBH) observations of the surface morphology of the anodic Hf treated by chronoamperometry at different potentials for 100 s.

3.3. Numerical Analysis

3.3.1. Determination of Anodic Corrosion Kinetic Parameters

The anodic Hf corrosion/dissolution reaction with kinetic control obeys the Butler–Volmer equation [19,21].

$$j = j_{corr}[\exp(\frac{ff_a zF(E - E_{eq})}{RT}) - \exp(-\frac{ff_c zF(E - E_{eq})}{RT})] \quad (1)$$

where j is the external current density, mA/cm^2; j_{corr} is the corrosion current density, mA/cm^2; T is the thermodynamic temperature, K; z is the number of electrons involved in the electrode reaction; F is the Faraday constant; R is the gas constant; α_a is the anodic charge transfer coefficient; α_c is the cathodic charge transfer coefficient; E is the electrode potential, V; and E_{eq} is the equilibrium potential, V.

At high anode potential, the current mainly comes from the anodic current, and the cathodic current can be negligible. Equation (1) follows the Tafel law [22] and can be simplified as follows:

$$J_a = E - E_{eq} = b_a \log|j| - b_a \log j_{corr} \quad b_a = \frac{\partial J_a}{\partial \log j} = \frac{2.303RT}{ff_a zF} \quad (2)$$

where b_a is the anodic Tafel slope, V dec^{-1}.

The corrosion current density (j_{corr}) and corrosion potential (E_{corr}) were evaluated from the intersection of the polarization curves' anodic and cathodic linear branches. According to Faraday's law, the corrosion rate is proportional to the corrosion current. Based on the anodic Hf corrosion current density, the Hf corrosion rate (v_{corr}) was determined through Equation (3) [23,24].

$$v_{corr} = 3269\, j_{corr} \frac{M}{n\,\rho} \quad (3)$$

where M is the atomic weight of Hf, 178.49 g/mol; n is the number of electrons transferred in the corrosion reaction, n = 4; and ρ is the density of Hf, 13.31 g/cm^3.

The log *j*–log *t* relationship based on chronoamperometry can be expressed as [24,25]:

$$\log\, j = A - m\, \log\, t \quad (4)$$

where A is the constant; m is the slope of log *j*–log *t*; m represents the parameters related to passive rate.

3.3.2. Linear Polarization Resistance Measurements

As the polarization potential ΔE is very small, the polarization curve E vs. i is approximately a straight line. By definition, the linear polarization resistance (R_p) is the slope of the polarization curve at overpotential ΔE = 0 V (or at corrosion potential E_{corr}), calculated based on the Stern–Geary equation [20].

$$R_p = \left[\frac{\Delta E}{\Delta i}\right]_{(\Delta E)\to 0} \quad (5)$$

where R_p is the polarization resistance given by $(\partial E/\partial i)_{\Delta E = 0}$.

4. Results and Discussion

4.1. Anodic Behavior of Hf in Et_4NCl-Based Anhydrous Ethanol System

The anodic Hf corrosion/dissolution behaviors in the tetraethylammonium chloride (Et_4NCl)-based EHS system were explored through cyclic voltammetry (CV) curves combined with SEM microscopy observation (Figure 3). The anodic Hf initially underwent a passive region with low current density due to the spontaneous formation of the hafnium oxide (HfO_2) passive film on the electrode surface [26]. When the positive sweep potential value reached a critical value (pitting potential, E_{pit}), the current density started increasing dramatically. This indicated that the passive film on the anodic Hf surface was broken down by the adsorbed Cl^- anions [27] and that the bare Hf metal was subject to an intense dissolution/corrosion reaction [28]. Subsequently, the potential started to reverse the scan, and the current density gradually decreased, forming a significant counter-clockwise hysteresis loop, the typical feature of the pitting corrosion [29]. Furthermore, as the potential scanning range expanded from −1~3 V to −1~5 V, the dissolution-potential (ΔE_{dis}) region expanded from 0.64 V to 1.56 V, which raised overall current density and shifted E_{pit} in a positive direction. This indicated a broad potential-current window for Hf electrodissolution in the practical operation of the EHS process, giving a significant improvement in potential tunability. SEM morphology demonstrated the pitting mechanism in the Hf electrodissolution process of the Et_4NCl-based anhydrous ethanol system and exhibited its pitting evolution trend [18]. For each pitting pit, the corrosion occurred in a nucleation center and propagated from inside toward the outside as the applied potential and corrosion time increased. At higher anodic potential, the pitting pits on the surface of the anodic Hf samples became deeper and larger, with their number surging.

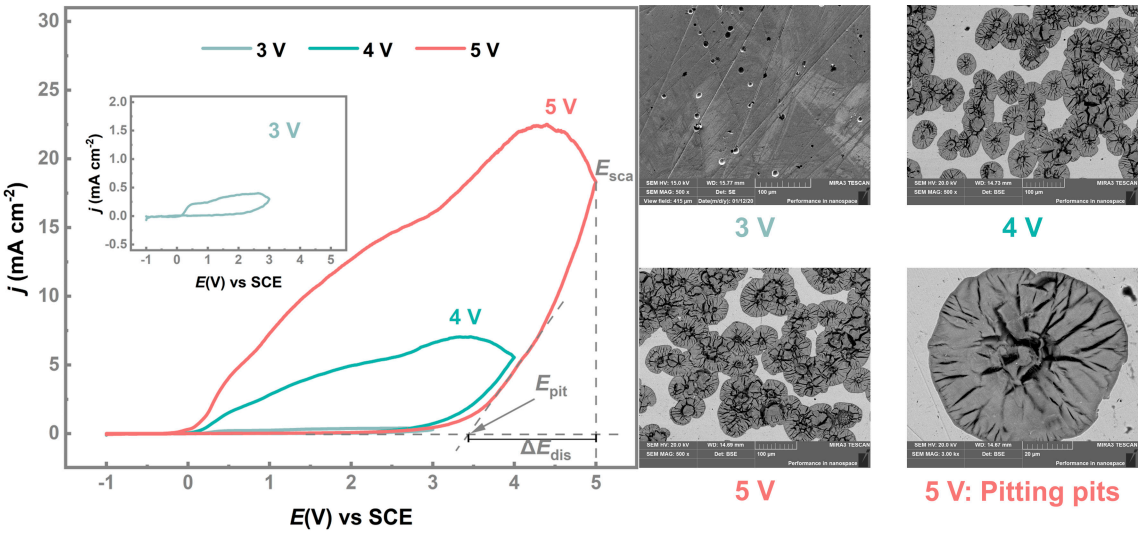

Figure 3. Cyclic voltammetry curves and SEM observation on anodic Hf corrosion in the Et_4NCl-based anhydrous ethanol system. Condition: on Hf in the ethanol and acetonitrile (V/V = 1:1) solution containing 0.06 M Et_4NCl at different potentials, 30 °C and a scanning rate of 1 mV/s. SEM images were obtained by chronoamperometry at different potentials for 100 s. $\Delta E_{dis} = E_{sca} - E_{pit}$.

To gain insights into the kinetics of the anodic Hf pitting mechanism in the Et_4NCl-based anhydrous ethanol system, we analyzed Tafel curves (Figure 4) to extract critical kinetic parameters such as anodic Tafel slope (b_a) and corrosion rate (v_{corr}) based on the Butler–Volmer equation. The results are recorded in Table 1. It is apparent from Figure 4 that the general shape of the Tafel polarization curve varied not with temperature and Et_4NCl concentration but only slightly shifted. As the temperature (25–35 °C) and Et_4NCl concentration (0.02–0.08 M) increased, the Tafel slope b_a decreased from 0.547 and 0.468 V dec^{-1}

to 0.273 and 0.296 V dec^{-1}, respectively. It can be seen from Equation (2) that the smaller the Tafel slope value, the faster the current density increased, indicating the promotion of anodic Hf pitting kinetics and the increase in pitting corrosion activity [30]. With the increase in temperature and Et_4NCl concentration from 25 °C and 0.02 M to 35 °C and 0.08 M, the corrosion rate v_{corr} increased from 6.38 and 5.56 μm y^{-1} to 8.55 and 8.79 μm y^{-1}, respectively. This indicated that higher temperature and Et_4NCl concentration facilitated Hf pitting kinetics and charge transfer, thus promoting the anodic Hf corrosion/dissolution.

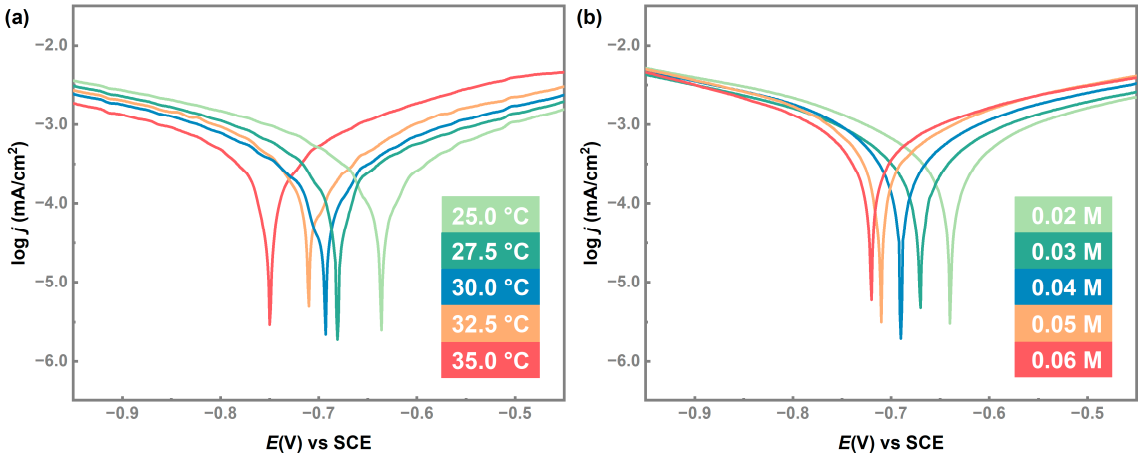

Figure 4. Tafel curves on Hf in the ethanol and acetonitrile (V/V = 1:1) solution. (**a**) Containing 0.06 M Et_4NCl at a scanning rate of 1 mV/s and different temperatures. (**b**) Containing different concentrations of Et_4NCl at a scanning rate of 1 mV/s and 30 °C.

Table 1. Reaction kinetic parameters of Hf anodic corrosion/dissolution in the Et_4NCl-based anhydrous ethanol system extracted from the Tafel curves. The kinetic parameters were calculated based on the Butler–Volmer equation. Condition: on Hf in the ethanol and acetonitrile (V/V = 1:1) solution. (a) Containing 0.06 M Et_4NCl at a scanning rate of 1 mV/s and different temperatures. (b) Containing different concentrations of Et_4NCl at a scanning rate of 1 mV/s and 30 °C.

(a) T/°C	b_a (V dec^{-1})	v_{corr} (μm y^{-1})	(b) C/M	b_a (V dec^{-1})	v_{corr} (μm y^{-1})
25.0	0.547	6.38	0.02	0.468	5.56
27.5	0.465	6.93	0.04	0.415	6.52
30.0	0.397	7.45	0.06	0.397	7.45
32.5	0.363	7.98	0.08	0.322	8.25
35.0	0.273	8.55	0.10	0.296	8.79

4.2. Anodic Behavior of Hf in Et_4NHSO_4-Based Anhydrous Ethanol System

The anodic corrosion/dissolution behaviors of Hf in the tetraethylammonium bisulfate (Et_4NHSO_4)-based EHS system were explored through CV curves and SEM observation (Figure 5). With scanning of the potential in a positive direction, the electrode process successively underwent a transition stage in which the current density increased to a steady-state value, a passivation stage in which the current density increased slowly, and a trans-passivation stage in which the current density increased relatively rapidly. Subsequently, the scanning potential was reversed, and the current density decreased without the appearance of a counter-clockwise hysteresis loop, indicating a different corrosion mechanism occurred in the Et_4NHSO_4 system compared with the Et_4NCl system. Note that the peak current density was lower than 0.05 mA/cm^2, due to the spontaneous formation of HfO_2 porous passive film that severely hindered the corrosion/dissolution of HSO_4^- ions on the Hf surface [17,31]. Hf corrosion could only occur behind the passive film, and its product traversed across the obstructive channels within the film into the electrolyte. SEM observation demonstrated the weak corrosion mechanism under the passive film in the Et_4NHSO_4 system, which showed trace corrosion evidence.

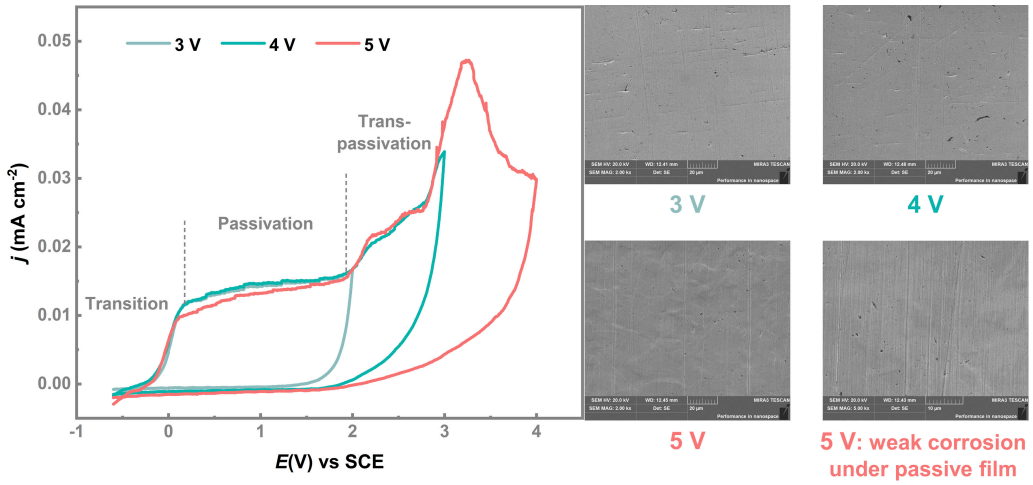

Figure 5. Cyclic voltammetry curves and SEM observations on anodic Hf corrosion in the Et_4NHSO_4-based anhydrous ethanol system. Condition: on Hf in the ethanol and acetonitrile (V/V = 1:1) solution containing 0.06 M Et_4NHSO_4 at different potentials, 30 °C and a scanning rate of 1 mV/s; SEM images were obtained by chronoamperometry at different potentials for 100 s.

Next, the anodic Hf dissolution/corrosion behaviors in the Et_4NHSO_4-based anhydrous ethanol system at constant anodic potential were investigated (Figure 6). The results showed that the current density dropped sharply to a "0 value" plateau, which reflected the formation, growth and compaction of the passive film under which weak anodic Hf corrosion occurred. The shape and trend of the current density (j)–time (t) curves did not change radically as the applied potential (E_{ap}) increased from 2.0 to 5.6 V, indicating an unchanged corrosion mechanism within this potential range. To quantify the effect of applied potentials (E_{ap}) on anodic Hf corrosion kinetics, we converted the j–t curves (Figure 6a) to the logarithmic scale (Figure 6b) and extracted the $|m|$ related to the passive rate based on Equation (4). As E_{ap} increased from 2.0 V to 5.6 V, $|m|$ decreased from 0.89 to 0.67, indicating that higher applied potential reduced the passive rate and benefited the corrosion/dissolution of the punctured bare Hf. This was due to the increasing adsorption of aggressive anions (HSO_4^-) on the surface of the passive film and the punctured bare metal [24,32]. The results were also consistent with the CV results that indicated the Hf corrosion can only occur under the passive film and its product traversed across the obstructive channels within the film into the electrolyte.

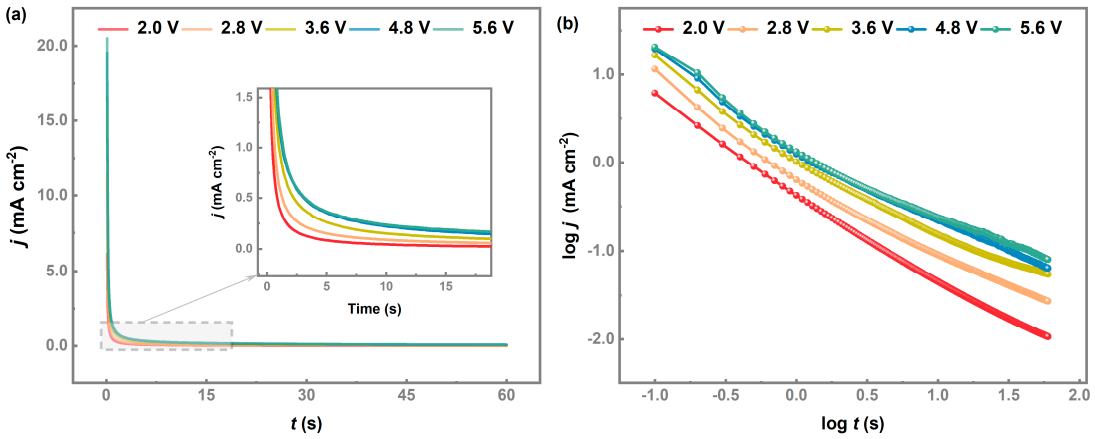

Figure 6. (**a**) Anodic transient current density (j) vs. time (t) curves; (**b**) Dependence of current density in logarithmic scale (log j) on the logarithmic scale of time (log t). Condition: on Hf in the ethanol and acetonitrile (V/V = 1:1) solution containing 0.06 M Et_4NHSO_4 at 30 °C and different anodic potentials.

4.3. Comparison between Hf Corrosion in Et_4NCl and Et_4NHSO_4 Systems by Polarization Resistance Analysis

Linear polarization resistance analysis has the advantages of requiring low polarized current density and causing weak interference on the measured system. It makes up for the shortcomings of the Tafel extrapolation method [33] that is applicable to an activation-controlled system and exerts strong polarization on the electrode being corroded, which easily damages the surface state of the sample and leads to inaccurate measurement results [34–36]. Thus, the linear polarization resistance method was employed to synthetically compare the anodic Hf corrosion/dissolution kinetics between Et_4NCl and Et_4NHSO_4 systems, and the results are shown in Figure 7. With increasing temperature from 25 °C to 35 °C, the polarization resistance of anodic Hf corrosion decreased from 130.89 kΩ cm^2 to 97.47 kΩ cm^2, which can be explained by the external conditions such as temperature, which improves the kinetics of anodic Hf corrosion/dissolution in the Et_4NCl system and thus has a facilitating effect on the charge transfer of the Hf pitting/dissolution reaction. The same pattern was shown in the Et_4NHSO_4 system, where the polarization resistance decreased from 555.56 kΩ cm^2 to 301.21 kΩ cm^2 as the temperature of the system increased from 25 °C to 35 °C. This was because the higher temperature favored the corrosion/dissolution of the adsorbed aggressive anion (HSO_4^-) on the passive film and the punctured bare metal, decreasing the kinetic barriers of the Hf corrosion/dissolution reaction. However, under the same conditions, the polarization resistance of the Et_4NHSO_4 system was 3–4 times greater than that of the Et_4NCl system, which indicated that the kinetic hindrance to anodic Hf corrosion/dissolution was at a lower level in the Et_4NCl system than in the Et_4NHSO_4 system, making it easier for Hf corrosion/dissolution to occur. It further confirmed that the Et_4NCl system had better anodic Hf corrosion performance than the Et_4NHSO_4 system.

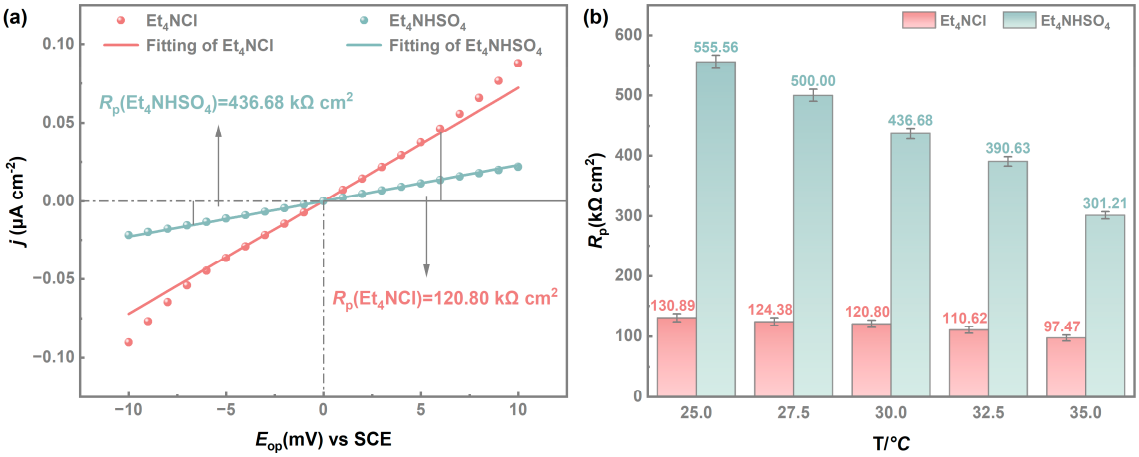

Figure 7. (**a**) Comparison of Hf corrosion in the Et_4NCl and Et_4NHSO_4 systems by polarization resistance analysis. (**b**) Polarization resistance kinetics of anodic Hf corrosion/dissolution in Et_4NCl and Et_4NHSO_4 based anhydrous ethanol systems. The polarization resistances were calculated based on the Stern–Geary equation. Condition: on Hf in the ethanol and acetonitrile (V/V = 1:1) solution containing 0.06 M Et_4NCl or Et_4NHSO_4 at a scanning rate of 1 mV/s and different temperatures.

5. Conclusions

The anodic Hf corrosion/dissolution electrochemical behaviors of the Et_4NCl and Et_4NHSO_4 based anhydrous systems were investigated through electrochemical measurements combined with SEM observations. This system, which employed green ethanol and Hf as feedstocks, was operated based on the simultaneous heterogeneous reactions of Hf dissolution and ethanol dehydrogenation, as well as the spontaneous solution-based reaction of Hf^{4+} and OR^-. The results demonstrated that the Et_4NCl system exhibited an efficient mechanism of passive film pitting corrosion breakdown and metal Hf dissolution. Important kinetic parameters such as anodic Tafel slope (b_a) and corrosion rate (v_{corr}) ex-

tracted based on the Butler–Volmer equation indicated that higher temperature and Et_4NCl concentration facilitated Hf pitting kinetics and charge transfer and increased the pitting corrosion activity, thus promoting the anodic Hf corrosion/dissolution. In contrast, the Et_4NHSO_4-based anhydrous ethanol system reflected the weak corrosion mechanism of the anodic Hf under the passive film. The $|m|$ related to the passive rate was extracted to quantify the anodic Hf corrosion kinetics. The results indicated that the increase in the applied potential E_{ap} enhanced the adsorption of aggressive anions (HSO_4^-) on the surface of the passive film, which exacerbated the dissolution of the passive film.

Furthermore, the effect mechanism of two typical supporting electrolytes, Et_4NCl and Et_4NHSO_4, on the anodic Hf corrosion/dissolution kinetics of the EHS system was synthetically estimated by adopting the linear polarization resistance method. The results demonstrated that the improvement in external conditions reduced the kinetic hindrance to anodic Hf corrosion/dissolution and thus facilitated the Hf corrosion/dissolution reaction. Under the same conditions, the polarization resistance of the Et_4NCl system was dramatically lower than that of the Et_4NHSO_4 system, which indicated that the kinetic hindrance to anodic Hf corrosion/dissolution was at a lower level in the Et_4NCl system than in the Et_4NHSO_4 system, making it easier for Hf corrosion/dissolution to occur. It further confirmed that the Et_4NCl system had better anodic Hf corrosion performance than the Et_4NHSO_4 system. Overall, the investigation of the electrochemical behaviors of anodic Hf corrosion/dissolution provides theoretical guidance for the efficient operation of EHS electrolysis and valuable reference significance for the utilization and high-value treatment of unconventional resources (hafnium, ethanol).

Author Contributions: Conceptualization, C.W.; methodology, C.W.; formal analysis, S.L.; investigation, S.L. and P.Z.; resources, S.Y.; writing—original draft preparation, S.L.; writing—review and editing, C.W. and S.L.; supervision, C.W.; funding acquisition, S.Y., Y.C., C.T., Y.L., C.D. and C.W. All authors have read and agreed to the published version of the manuscript.

Funding: This research was funded by the science and technology innovation Program of Hunan Province (No.2021RC2002) and the Yangfan Plan (No.2017YT05C107).

Institutional Review Board Statement: Not applicable.

Informed Consent Statement: Not applicable.

Data Availability Statement: Not applicable.

Conflicts of Interest: The authors declare no conflict of interest.

References

1. Suzuki, R.; Taoka, N.; Yokoyama, M.; Lee, S.; Kim, S.; Hoshii, T.; Yasuda, T.; Jevasuwan, W.; Maeda, T.; Ichikawa, O.; et al. 1-nm-capacitance-equivalent-thickness HfO_2/Al_2O_3/InGaAs metal-oxide-semiconductor structure with low interface trap density and low gate leakage current density. *Appl. Phys. Lett.* **2012**, *100*, 132906. [CrossRef]
2. Kang, Y.; Kim, C.; Cho, M.-H.; Chung, K.; An, C.-H.; Kim, H.; Lee, H.; Kim, C.; Lee, T. Thickness dependence on crystalline structure and interfacial reactions in HfO_2 films on InP (001) grown by atomic layer deposition. *Appl. Phys. Lett.* **2010**, *97*, 172108. [CrossRef]
3. Kang, Y.; Kim, C.; Cho, M.; An, C.; Kim, H.; Seo, J.; Kim, C.; Lee, T.; Ko, D. Interfacial Reactions between HfO_2 Films Prepared by Atomic-Layer-Deposition and an InP Substrate Using Postnitridation with NH_3 Vapor. *Electrochem. Solid-State Lett.* **2012**, *15*, G9. [CrossRef]
4. Zhang, S.; Northrup, J. Chemical potential dependence of defect formation energies in GaAs: Application to Ga self-diffusion. *Phys. Rev. Lett.* **1991**, *67*, 2339–2342. [CrossRef] [PubMed]
5. Timm, R.; Head, A.R.; Yngman, S.; Knutsson, J.V.; Hjort, M.; McKibbin, S.R.; Troian, A.; Persson, O.; Urpelainen, S.; Knudsen, J.; et al. Self-cleaning and surface chemical reactions during hafnium dioxide atomic layer deposition on indium arsenide. *Nat. Commun.* **2018**, *9*, 1412. [CrossRef]
6. Gordon, R.G.; Becker, J.; Hausmann, D.; Suh, S. Vapor Deposition of Metal Oxides and Silicates: Possible Gate Insulators for Future Microelectronics. *Chem. Mater.* **2001**, *13*, 2463–2464. [CrossRef]
7. Hausmann, D.M.; Kim, E.; Becker, J.; Gordon, R.G. Atomic Layer Deposition of Hafnium and Zirconium Oxides Using Metal Amide Precursors. *Chem. Mater* **2002**, *14*, 4350–4358. [CrossRef]

8. Miikkulainen, V.; Leskelä, M.; Ritala, M.; Puurunen, R.L. Crystallinity of inorganic films grown by atomic layer deposition: Overview and general trends. *J. Appl. Phys* **2013**, *113*, 021301. [CrossRef]
9. Mui, C.; Musgrave, C.B. Atomic Layer Deposition of HfO_2 Using Alkoxides as Precursors. *J. Phys. Chem. B* **2004**, *108*, 15150–15164. [CrossRef]
10. Bradley, D.; Mehrotra, R.C.; Rothwell, I.; Singh, A. *Alkoxo and Aryloxo Derivatives of Metals*; Elsevier: Amsterdam, The Netherlands, 2001.
11. Artz, J.; Müller, T.E.; Thenert, K.; Kleinekorte, J.; Meys, R.; Sternberg, A.; Bardow, A.; Leitner, W. Sustainable Conversion of Carbon Dioxide: An Integrated Review of Catalysis and Life Cycle Assessment. *Chem. Rev.* **2018**, *118*, 434–504. [CrossRef]
12. Peng, R. *Metallurgy of Heavy Metals*; Central South University Press: Changsha, China, 2004.
13. Li, Y.G.; Liu, S.S.; Wang, C.H.; Luo, T.; Xiang, C.L.; Li, S.; Chang, C.; Yang, S.H.; Wang, H.H.; Chen, Y.M. Electro-Deposition Behavior in Methanesulfonic-Acid-Based Lead Electro-Refining. *J. Sustain. Metall* **2021**, *7*, 1910–1916. [CrossRef]
14. Turner, J.A. A Realizable Renewable Energy Future. *Science* **1999**, *285*, 687–689. [CrossRef] [PubMed]
15. Glenk, G.; Reichelstein, S. Economics of converting renewable power to hydrogen. *Nat. Energy* **2019**, *4*, 216–222. [CrossRef]
16. Sharifian, R.; Wagterveld, R.M.; Digdaya, I.A.; Xiang, C.; Vermaas, D.A. Electrochemical carbon dioxide capture to close the carbon cycle. *Energy Environ. Sci.* **2021**, *14*, 781–814. [CrossRef]
17. Li, S.; Yang, S.; Wang, C. Electrochemical Behavior of Tetraethylammonium-Hydrogen Sulfate-Based Electrodissolution-Coupled Hafnium Alkoxide Synthesis. *JOM* **2022**, *74*, 3548–3556. [CrossRef]
18. Li, S.; Yang, S.; Li, K.; Lai, Y.; Deng, C.; Wang, C. Electrodissolution-Coupled Hafnium Alkoxide Synthesis with High Environmental and Economic Benefits. *ChemSusChem* **2022**, *15*, e202200474. [CrossRef]
19. Bard, A.J.; Faulkner, L.R. *Electrochemical Methods: Fundamentals and Applications*; John Wiley & Sons, Inc.: New York, NY, USA, 1980.
20. Stern, M.; Geary, A.L. Electrochemical Polarization: I. A Theoretical Analysis of the Shape of Polarization Curves. *J. Electrochem. Soc.* **1957**, *104*, 56. [CrossRef]
21. Bockris, J.O.M.; Reddy, A.K.N. *Modern Electrochemistry*; Springer: Boston, MA, USA, 1970; Volume 2.
22. Tafel, J. Über die Polarisation bei kathodischer Wasserstoffentwicklung. *Z. Phys. Chem.* **1905**, *50*, 641–712. [CrossRef]
23. Prasai, D.; Tuberquia, J.C.; Harl, R.R.; Jennings, G.K.; Bolotin, K.I. Graphene: Corrosion-Inhibiting Coating. *ACS Nano* **2012**, *6*, 1102–1108. [CrossRef] [PubMed]
24. Amin, M.A. Uniform and pitting corrosion events induced by SCN− anions on Al alloys surfaces and the effect of UV light. *Electrochim. Acta* **2011**, *56*, 2518–2531. [CrossRef]
25. Lin, L.F.; Chao, C.Y.; Macdonald, D.D. A Point Defect Model for Anodic Passive Films: II. Chemical Breakdown and Pit Initiation. *J. Electrochem. Soc.* **1981**, *128*, 1194–1198. [CrossRef]
26. Wang, C.; Yang, S.; Yuan, Y.; Chen, Y.; Wang, B.; He, J.; Tang, C. Corrosion behavior of hafnium in anhydrous isopropanol and acetonitrile solutions containing bromide ions. *Trans. Nonferrous Met. Soc. China* **2017**, *27*, 1896–1906. [CrossRef]
27. Li, S.; Yang, S.; Chen, Y.; Tang, C.; Lai, Y.; Deng, C.; Wang, C. Electrochemical mechanism and kinetics of electrodissolution-coupled hafnium alkoxide synthesis in a tetraethylammonium-chloride-based anhydrous system. *Trans. Nonferrous Met. Soc. China*, 2023; submitted for publication.
28. Wang, C.H.; Yang, S.H.; Chen, Y.M.; Wang, B.; He, J.; Tang, C.B. Effect of bromide ions on the corrosion behavior of hafnium in anhydrous ethanol. *RSC Adv.* **2015**, *5*, 34580–34587. [CrossRef]
29. Wang, C.H.; Yang, S.H.; Chen, Y.M.; Yang, X.Y.; Wang, B.; He, J.; Tang, C.B. Electrochemical Behaviour of Hafnium in Anhydrous n-butanol Containing Tetraethylammonium Bromide. *Int. J. Electrochem. Sci.* **2017**, *12*, 545–560. [CrossRef]
30. Zhao, G.; Rui, K.; Dou, S.X.; Sun, W. Heterostructures for Electrochemical Hydrogen Evolution Reaction: A Review. *Adv. Funct. Mater.* **2018**, *28*, 1803291. [CrossRef]
31. Wang, C.; Jiang, K.; Yu, H.; Yang, S.; Li, K. Copper electrowinning-coupled CO_2 capture in solvent based post-combustion capture. *Appl. Energy* **2022**, *316*, 119086. [CrossRef]
32. Amin, M.A. A newly synthesized glycine derivative to control uniform and pitting corrosion processes of Al induced by SCN—anions—Chemical, electrochemical and morphological studies. *Corros. Sci.* **2010**, *52*, 3243–3257. [CrossRef]
33. Wang, C.H.; Jiang, K.Q.; Jones, T.W.; Yang, S.H.; Yu, H.; Feron, P.; Li, K.K. Electrowinning-coupled CO_2 capture with energy-efficient absorbent regeneration: Towards practical application. *Chem. Eng. J.* **2022**, *427*, 131981. [CrossRef]
34. Scully, J.R. Polarization Resistance Method for Determination of Instantaneous Corrosion Rates. *Corrosion* **2000**, *56*, 3548–3556. [CrossRef]
35. Wang, C.; Li, K.; Yu, H.; Yang, S.; Jiang, K. Electrochemical behavior of Cu-mediated electrowinning-coupled CO_2 capture. *Electrochim. Acta* **2022**, *422*, 140571. [CrossRef]
36. Xiang, C.; Zhu, S.; Song, J.; Li, Y.; Luo, T.; Chang, C.; Qu, J.; Yang, S.; Wang, C.; Chen, Y. Green Electrorefining of Crude Lead with High-Quality Deposits in an Additive-Assisted Methanesulfonic Acid System. *ACS Sustain. Chem. Eng.* **2022**, *10*, 11223–11231. [CrossRef]